

# Novel p–p Heterojunctions Self-Powered Broadband Photodetectors with Ultrafast Speed and High Responsivity

Pingping Yu, Kai Hu, Hongyu Chen, Lingxia Zheng, and Xiaosheng Fang\*

Novel inorganic/organic self-powered UV–vis photodetectors based on single Se microtube and conducting polymers—polyaniline (PANI), polypyrrole (PPy), and poly(3,4-ethylenedioxythiophene) (PEDOT)—are fabricated. The conducting polymers are directly coated on the surface of a single Se microtube via a facile and low-cost in situ polymerization method. The integrated Se/PANI photodetector with 45-nm-thick PANI layer shows excellent self-powered behavior under UV–vis light illumination. In particular, it exhibits high on/off ratio of  $1.1 \times 10^3$ , responsivity ( $120 \text{ mA W}^{-1}$ ), large detectivity ( $3.78 \times 10^{11}$  Jones), and ultrafast response speed (rise time of  $4.5 \mu\text{s}$  and fall time of  $2.84 \text{ ms}$ ) at zero bias at  $610 \text{ nm}$  ( $0.434 \text{ mW cm}^{-2}$ )-light illumination. Moreover, the individual Se/PPy and Se/PEDOT self-powered photodetectors also exhibit fast and stable responses, including responsivity of  $70$  and  $5.5 \text{ mA W}^{-1}$ , rise time of  $0.35$  and  $1.00 \text{ ms}$ , fall time of  $16.97$  and  $9.78 \text{ ms}$ , respectively. Given the simple device architecture and low cost fabrication process, this work provides a promising way to fabricate inorganic/organic, high-performance, self-powered photodetectors.

## 1. Introduction

Self-powered photodetectors (PDs) have attracted considerable attention in the information age, showing promising applications in image sensing, optical communications, environmental monitoring, and industrial security.<sup>[1–3]</sup> Compared with the traditional PDs, the designed self-powered structures such as p–n junctions, heterojunctions, Schottky junctions, and organic/inorganic hybrid junctions can quickly separate the electron–hole pairs by a built-in electric field, which exhibits faster photoresponse speed and higher photosensitivity at zero bias.<sup>[4–7]</sup> However, these self-powered PDs possess many requirements on hybrid materials and device processing techniques, leading to high cost and complicated processing to limit the practical applications. Therefore, the high quality and stable self-powered PDs fabricated by a facile and low cost way is necessary to improve their performance.


The organic/inorganic hybrid junctions can provide a promising route to combine the broadband absorption and

the excellent intrinsic carrier mobility of inorganic-based devices, as well as tunable functionality and easy formation properties of organic based devices.<sup>[8–10]</sup> Conducting polymers including polyaniline (PANI), polypyrrole (PPy), and poly(3,4-ethylenedioxythiophene) (PEDOT) are the highly  $\pi$ -conjugated organic polymers, which show wide applications in sensors, supercapacitors, dye sensitized solar cells,<sup>[11]</sup> light emitting diodes, and photodetectors.<sup>[11–14]</sup> They possess interesting properties such as low cost, easy synthesis, tunable nature, conjugated  $\pi$ -electrons in the polymer backbone and high stability. In particular, PANI can change conduction by protonation of the emeraldine base (EB) to form charged structure emeraldine salt (ES) by acid–base chemistry, leading to the tunable bandgaps.<sup>[15]</sup> The optical absorptions of EB at about  $2$  and  $3.5 \text{ eV}$  differ from that of ES at about  $1.5$ ,  $3.0$ , and

$4.1 \text{ eV}$ .<sup>[16,17]</sup> Recently, p-type conducting polymers in junction with n-type inorganic semiconductors such as Si,<sup>[18]</sup> ZnO,<sup>[19–21]</sup> ZnGa<sub>2</sub>O<sub>4</sub>,<sup>[22]</sup> SnO<sub>2</sub>,<sup>[6]</sup> CdSe,<sup>[23]</sup> and TiO<sub>2</sub><sup>[24,25]</sup> have been fabricated as the self-powered photoelectric devices due to p–n organic/inorganic heterojunctions. However, the conducting polymers layer is usually coated by physical blending or electrochemical deposition in neutral electrolyte to lose their electrical conductivity.<sup>[15–17]</sup> The proper doping agent for conducting polymers can provide tunable energy gap and charge carrier mobility, enhanced visible light absorption, and separation of photogenerated electron–hole pairs. Thus, an effective method to prepare highly doped conducting polymers and appropriate inorganic semiconductor for fabricating high photoresponse performance self-powered PDs is an urgent issue.

Among the inorganic semiconductors, p-type semiconductor selenium (Se) exhibits many unique physical properties including a relatively low melting point ( $\approx 490 \text{ K}$ ), high photoconductivity ( $8 \times 10^4 \text{ S cm}^{-1}$ ), and large thermoelectric, piezoelectric, and nonlinear optical responses.<sup>[26–29]</sup> Recently, a single trigonal Se microtube (t-Se-MT) PD fabricated by Hu et al. shows the peak responsivity of  $\approx 19 \text{ mA W}^{-1}$  at  $610 \text{ nm}$  and fast response speed (rise time of  $0.32 \text{ ms}$  and fall time of  $23.02 \text{ ms}$ ) in UV–vis region.<sup>[30]</sup> It demonstrated that Se microstructures synthesized by vapor phase deposition were easy to build PD device which showed fast response time and broadband photoresponsivity. In addition, the t-Se nanostructures can be very stable without any degradation in the dilute acid solution (ascorbic acid and H<sub>2</sub>SeO<sub>3</sub>) and form a core/shell structure

Dr. P. P. Yu, K. Hu, Dr. H. Y. Chen, Dr. L. X. Zheng, Prof. X. S. Fang  
Department of Materials Science  
Fudan University  
Shanghai 200433, China  
E-mail: xshfang@fudan.edu.cn

 The ORCID identification number(s) for the author(s) of this article can be found under <https://doi.org/10.1002/adfm.201703166>.

DOI: 10.1002/adfm.201703166

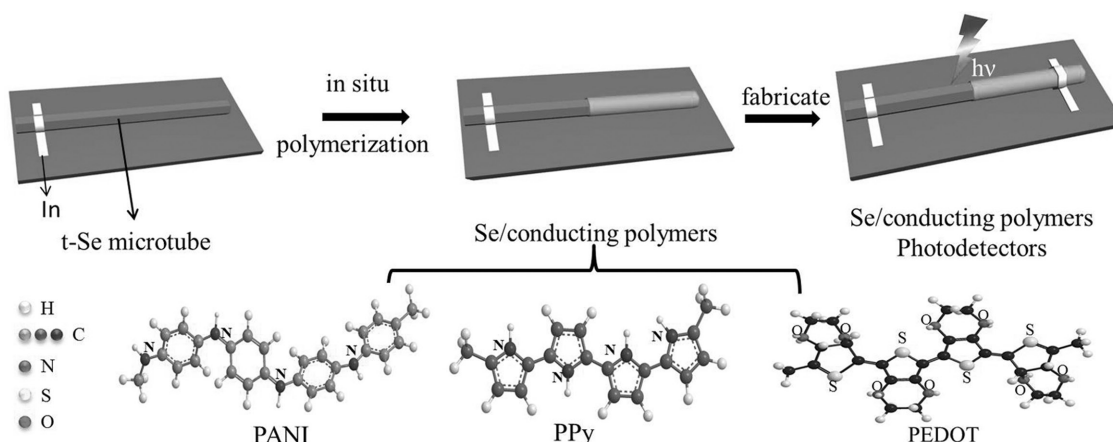


**Figure 1.** Schematic illustration of the fabrication process for the Se/conducting polymers (PANI, PPy, and PEDOT) heterojunctions photodetectors.

(Graphene@Se/PANI),<sup>[26,28,29]</sup> which benefited the fabrication of organic/inorganic heterojunctions. Therefore, t-Se-MT is a good candidate for incorporating with p-type conducting polymer semiconductors to design the self-powered PD devices.

In this paper, we report the fabrication of self-powered PDs employing individual t-Se microtube/conducting polymer p-p heterojunctions. The highly doped PANI, PPy, and PEDOT are directly grown on t-Se-MT surface in an acid aqueous solution by in situ polymerization as shown in **Figure 1**. The Se/PANI, Se/PPy, and Se/PEDOT heterojunctions are constructed into PD devices using Indium as the electrodes. These devices show broadband photoresponse range of 300–700 nm, fast response speed (rise time <1.0 ms and fall time <16.97 ms) at zero bias voltage with maximum peak responsivity of 120 mA W<sup>-1</sup> at 610 nm, which highlights the great potential of conducting polymers for construction of advanced organic/inorganic photoresponse devices.

## 2. Results and Discussion

**Figure 2a,b** shows the different magnification scanning electron microscopy (SEM) images of the as-prepared trigonal Se microtubes (t-Se-MTs) via a vapor transport and deposition method, demonstrating that a large quantity of freestanding microtubes with smooth and neat surface. The diameter of t-Se-MTs is mainly about 2–8 μm with a proportion of 60% and 8–14 μm with a proportion of 40%, and the length of t-Se-MTs is tens and hundreds of micrometers. **Figure 2c** reveals that t-Se-MTs show a hollow tubular morphology and pseudo-hexagon shape cross-section. For manual operation, the t-Se-MTs with larger diameter and longer length were chosen to fabricate organic/inorganic composites. The well-ordered PANI nanorods with average diameter of 20 nm and length of 50 nm are uniformly grown on the surface of t-Se-MT (**Figure 2d,e**). For Se/PPy (**Figure 2g,h**) and Se/PEDOT (**Figure 2j,k**), different surface morphologies are observed under the same experimental condition. Lots of PPy and PEDOT nanoparticles are formed into very thin and dense films on the surface of t-Se-MTs, similarly to the structure morphologies of pure PPy and PEDOT (**Figure S1**, Supporting Information). The thickness of PANI, PPy, and

PEDOT layer is ≈45, 60, and 108 nm for Se/PANI (**Figure 2f**), Se/PPy (**Figure 2i**), and Se/PEDOT (**Figure 2l**) heterojunctions, respectively.

**Figure 3a** shows the X-ray diffraction (XRD) patterns of t-Se-MT, Se/PANI, Se/PPy, and Se/PEDOT heterojunctions. The sharp and strong diffraction peaks can be indexed to trigonal selenium (t-Se, JCPDS No. 65-1876) with the lattice parameters of  $a = b = 4.364 \text{ \AA}$  and  $c = 4.959 \text{ \AA}$ , demonstrating good crystallinity.<sup>[31]</sup> As for Se/PANI, Se/PPy, and Se/PEDOT, similar diffraction peaks of t-Se-MT can be observed without the signals for PANI, PPy, and PEDOT (**Figure S2a**, Supporting Information), indicating that the integration of PANI, PPy, and PEDOT has little changing effect on the crystallinity of t-Se-MT. Raman spectroscopy provides further evidence that the conducting polymers are successfully coated on the t-Se-MT to form the p-p heterojunctions as shown in **Figure 3b**. An intense resonant peak at 236.6 cm<sup>-1</sup> is the characteristic signal of t-Se-MT in the trigonal phase, which can be attributed to the vibration of helical selenium chain.<sup>[32]</sup> For sample Se/PANI, apart from the 236.6 cm<sup>-1</sup> peak, the distinct peaks located at 1175, 1355, 1479, and 1593 cm<sup>-1</sup> are assigned to C–H bending of quinoid ring, C–N<sup>+</sup> stretching vibration, C=N stretching of the quinoid ring, and C–C stretching of benzene ring, respectively, suggesting the incorporation of highly electrical conductive PANI.<sup>[33,34]</sup> The peaks at around 522 and 574 cm<sup>-1</sup> can be attributed to amine deformation and ring deformation, respectively.<sup>[35]</sup> The new bands centered at 947, 1044, 1382, and 1583 cm<sup>-1</sup> for Se/PPy are ascribed to the ring stretching, C–H in-plane deformation, C–N stretching, and backbone stretching mode of C=C bonds of the oxidized species of PPy, respectively.<sup>[36,37]</sup> For Se/PEDOT, the bands at ≈995 and 878 cm<sup>-1</sup> are assigned to C–S bond in the oxyethylene ring, while the bands located at 1510 and 1438 cm<sup>-1</sup> are attributed to the C=C stretching of PEDOT.<sup>[38,39]</sup> **Figure 3c** presents the UV–vis absorption spectra in the range of 300–700 nm for Se/PANI, Se/PPy, and Se/PEDOT, which exhibits very similar absorption spectra to that of the t-Se-MTs. The absorption intensity increases from 300 to 700 nm, especially the greatly enhancement within visible range (500–700 nm), suggesting improved generation of electron-hole pairs after conducting polymers coating on t-Se-MT. The UV–vis absorption spectra for pure conducting polymers are

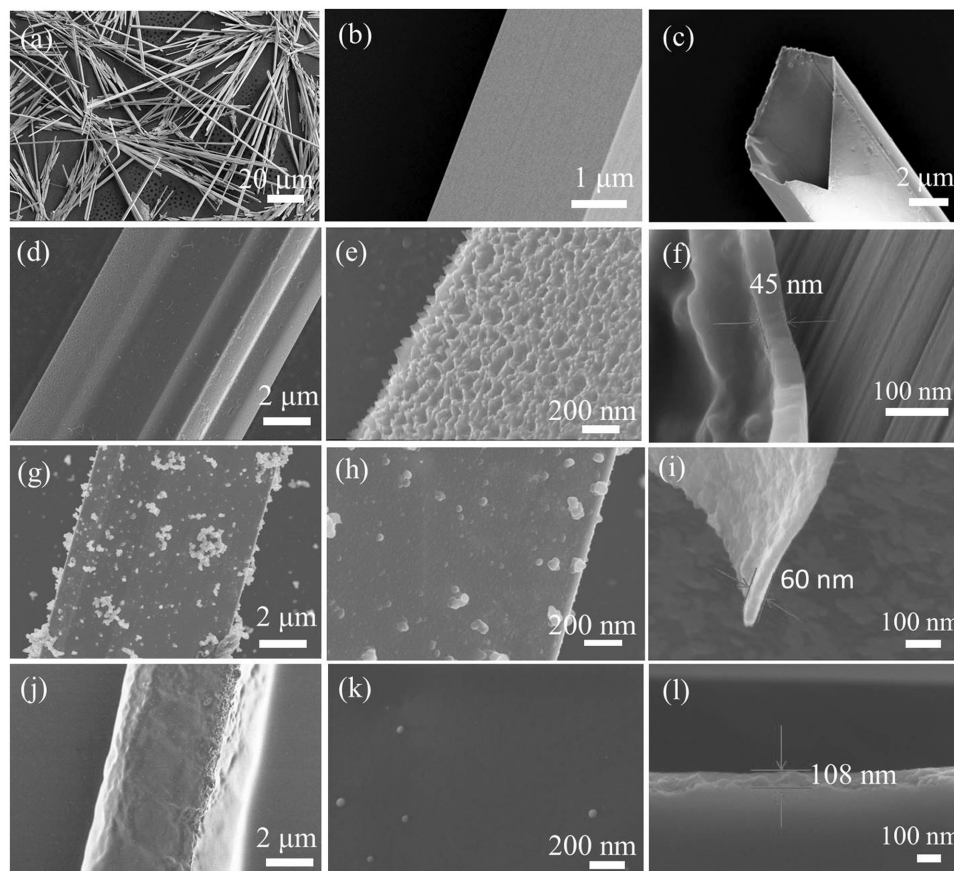


**Figure 2.** SEM images of a–c) t-Se-MT, d–f) Se/PANI, g–i) Se/PPy, and j–l) Se/PEDOT.

displayed in Figure 3d. The characteristic absorption peaks located at wavelength of  $\approx 330$ , 450, and 700 nm are assigned to the  $\pi$ - $\pi^*$  transition of the benzenoid rings,  $\pi$  to the localized polaron band and the exciton absorption of the quinoid rings, respectively.<sup>[40,41]</sup> The broad absorption band at about 500 nm for PPy is attributed to the transition from the valence band to the conduction band.<sup>[42]</sup> Pure PEDOT shows broad absorption peaks starting from 450 to 700 nm, which assigned to  $\pi$ - $\pi^*$  transition of the thiophene ring.<sup>[43]</sup> The peaks suggest the conducting state of conducting polymers.<sup>[44–46]</sup> Therefore, the very thin conducting polymers layers (45–108 nm) synthesized by in situ polymerization not only change the absorption characteristic of t-Se-MT but also enhance the absorption intensities.

The quality and surface composition are further measured by X-ray photoelectron spectroscopy (XPS) of the t-Se-MT, Se/PANI, Se/PPy, and Se/PEDOT in Figure 4. The XPS survey spectra are shown in Figure S2b in the Supporting Information, typical Se 3d, S 2p, C 1s, and N 1s signals can be seen, indicating the presence of PEDOT, PPy, and PANI in the heterojunctions. The binding energy of Se 3d at 54.9 eV (Figure 4a) for t-Se-MT confirms that Se is in its elemental state. The N 1s signals are deconvoluted to three peaks in Figure 4b,c for Se/PANI and Se/PPy, which are related to imine nitrogen ( $-N=$ ), amine nitrogen ( $-NH-$ ), and nitrogen cationic radical ( $-N^+-$ ) with binding energies located at 398.4, 399.8, and 401.5 eV for Se/PANI and 398.1, 399.4, and 401.2 eV for Se/PPy,

suggesting the doped PANI and PPy.<sup>[38]</sup> The high resolution S 2p spectrum of Se/PEDOT shows that (Figure 4d) the sulfur spin-split doublets at around 164.1 and 165.1 eV correspond to S 2p<sub>3/2</sub> and S 2p<sub>1/2</sub> states, respectively. The binding energy at 170.1 eV is ascribed to partially oxidized S<sup>δ+</sup> due to the incorporation of counterion HSO<sub>4</sub><sup>-</sup> into PEDOT, indicating the highly doped PEDOT.<sup>[47,48]</sup> The results suggest the successful coating of the conducting polymers on t-Se-MT.

In order to study the optoelectronic characteristics of the Se/conducting polymers heterojunctions, the photodetectors based on individual Se/PANI, Se/PPy, and Se/PEDOT were manually fabricated by using indium as the electrodes as described in Figure 1. The schematic illustration of Se/conducting polymers photodetector on a glass substrate is shown in Figure 5a. The two indium electrodes with 10 μm gap were deposited on the end of t-Se-MT and Se/conducting polymers composites. Figure 5b depicts the current–voltage (*I*-*V*) characteristics of the individual Se/PANI PD in dark and under different wavelength of 300-nm- (0.403 mW cm<sup>-2</sup>), 450-nm- (1.003 mW cm<sup>-2</sup>), and 610-nm- (0.434 mW cm<sup>-2</sup>) light illumination at room temperature, respectively. Note that the Se/PANI device in dark exhibits rectifying behavior with a rectifying ratio of  $30 \pm 5$ . Compared to those under 300 and 610 nm light irradiations, the *I*-*V* curves under the 450 nm blue light illumination display higher response, especially in the reverse bias. The *I*-*V* curves of pristine t-Se-MT (Figure S3a, Supporting Information)

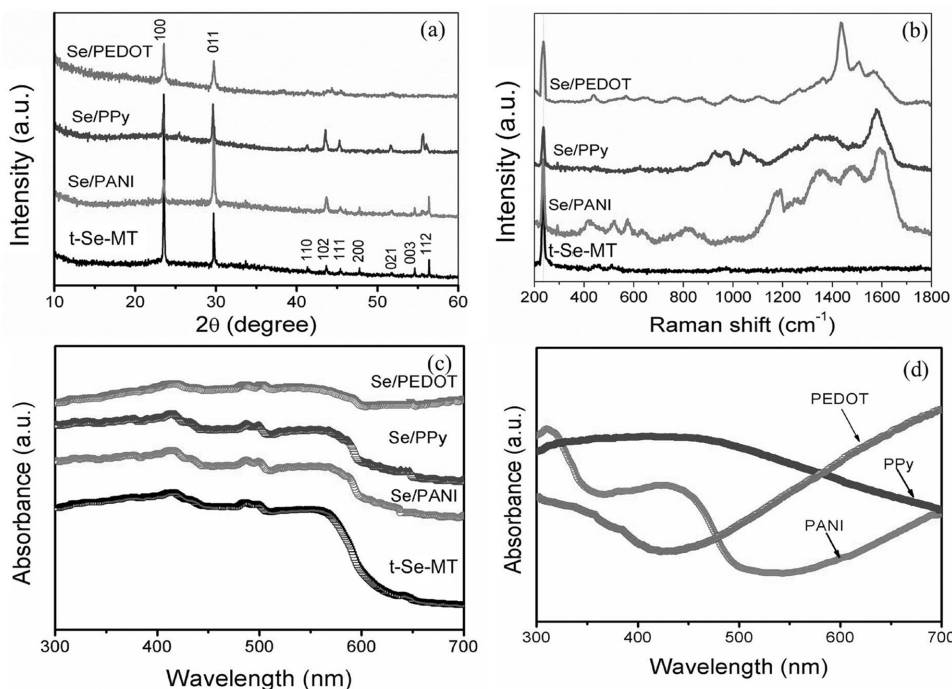


**Figure 3.** a) XRD patterns, b) Raman spectra, and c) UV-vis absorbance of t-Se-MT, Se/PANI, Se/PPy, and Se/PEDOT. d) UV-vis absorbance of pure PANI, PPy, and PEDOT.

and PANI PD devices (Figure S3b, Supporting Information) under dark and light illumination show linear characteristics, indicating that the t-Se-MT and pure PANI devices have good Ohmic contacts. The results demonstrate that the typical

photodiode behavior comes from the p-p heterojunction other than the metal-semiconductor contacts. The inset of Figure 5b shows the significant photovoltaic effect of the device under 610-nm-light illumination near zero bias, which provides an

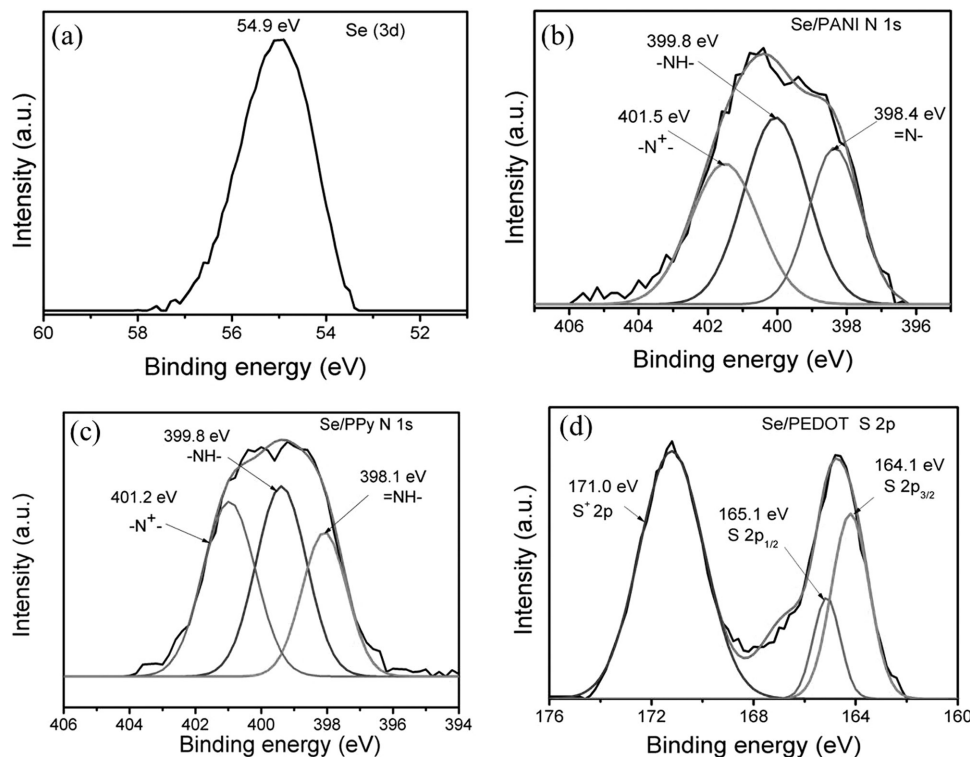


**Figure 4.** a) Se 3d spectra of t-Se-MT, b) N 1s XPS spectra of Se/PANI, and c) Se/PPy, d) S 2p XPS spectra of Se/PEDOT.

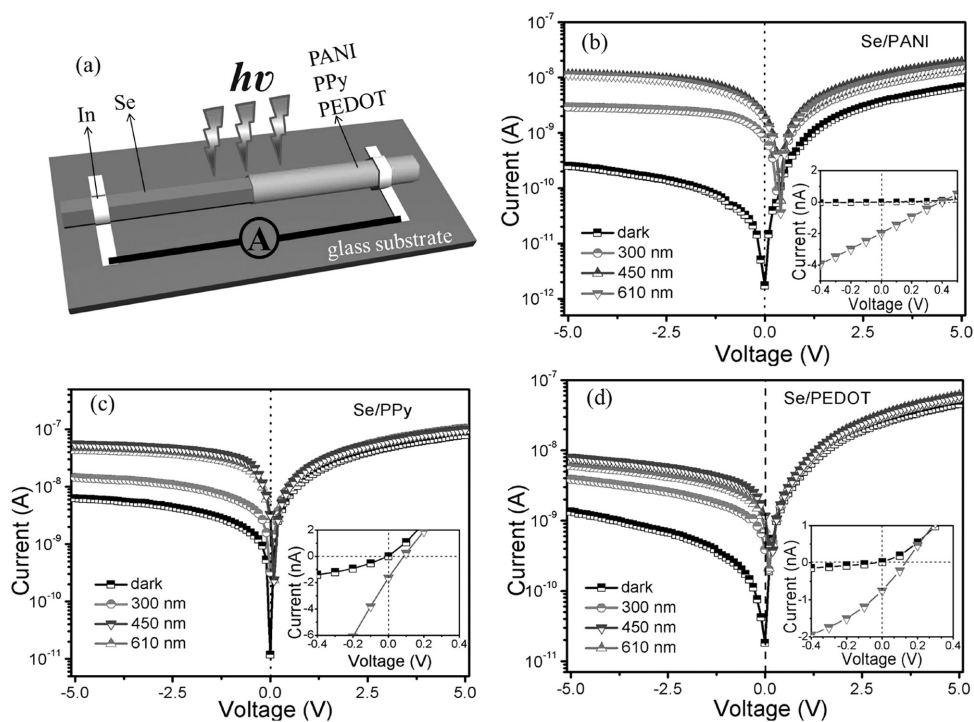


**Figure 5.** a) Schematic diagram of the device structure.  $I$ - $V$  characteristics of b) Se/PANI, c) Se/PPy, and d) Se/PEDOT PD in the dark and under the 300 nm ( $0.403 \text{ mW cm}^{-2}$ ), 450 nm ( $1.003 \text{ mW cm}^{-2}$ ), and 610 nm ( $0.434 \text{ mW cm}^{-2}$ ) illumination. The insets of (b)–(d) show the photovoltaic characteristic of the devices near zero bias at 610 nm.

open-circuit voltage  $V_{oc} = 0.40 \text{ V}$  and a short-circuit current of  $2.62 \text{ nA}$ , respectively. For pure PANI PD, the same current value under dark and 610-nm-light illumination indicates no photoresponse characteristics, due to photoexcited electron and hole recombination on a millisecond time scale.<sup>[49]</sup> Therefore, the as-fabricated Se/PANI PD is a broadband self-powered device which can be operated without any external power supply, since the built-in potential acts as the driving force to separate the electrons–hole pairs. Moreover, no photoresponse can be observed under 610-nm-light illumination for the pure PPy and PEDOT devices (Figure S3c,d, Supporting Information). The  $I$ - $V$  curves (Figure 5c,d) of individual Se/PPy and Se/PEDOT PDs show similar rectifier phenomena and self-powered characteristics to that of Se/PANI PD. It is also noteworthy that smaller values of  $V_{oc}$  under 610-nm-light illumination are observed for Se/PPy PD ( $V_{oc} = 0.12 \text{ V}$ ; the inset of Figure 5c) and Se/PEDOT PD ( $V_{oc} = 0.10 \text{ V}$ ; the inset of Figure 5d), indicating a weaker built-in electric field by organic/inorganic p–p heterojunctions.

The photoresponse speed and reproducibility of photoresponse are important parameters in the characterization of photodetectors. Figure 6a–c shows the photocurrent ( $I_{ph}$ ) response curves of three different kinds of PDs based on single Se/PANI, Se/PPy, and Se/PEDOT structure irradiated with 300, 450, and 610 nm light at zero bias voltage, respectively. The current–time ( $I$ - $t$ ) characteristics exhibit rapid photoresponse and good stability without noticeable photocurrent-decay of the three devices. The photocurrents of the three devices increase quickly to reach a steady state and then decrease rapidly when the light is switched on and off, indicating a rapid separation of

electron–hole near the p–p heterojunctions. For the Se/PANI PD (Figure 6a), the ratio of photocurrent to dark current ( $I_{ph}/I_d$ ,  $I_d \approx 2 \text{ pA}$ ) is estimated to be  $8 \times 10^2$ ,  $1.3 \times 10^3$ , and  $1.1 \times 10^3$  for 300-, 450-, and 610-nm-light illumination, respectively. The photocurrent values at 610 nm slightly decrease for Se/PPy ( $1.8 \text{ nA}$ ) and Se/PEDOT ( $1.05 \text{ nA}$ ) PD (Table 1) due to the lower  $V_{oc}$  values and weaker self-powered characteristic, consistent with the  $I$ - $V$  curves (Figure 5c,d). Compared to the Se/PANI device, the Se/PPy (Figure 6b) and Se/PEDOT PDs (Figure 6c) have much lower  $I_{ph}/I_d$  ratio of  $2.2 \times 10^2$  and 50, respectively, resulting from the higher dark current for PPy ( $I_d \approx 14 \text{ pA}$ ) and PEDOT ( $I_d \approx 20 \text{ pA}$ ). In order to measure the accurate response time of the inorganic/organic hybrid devices, a pulsed Nd:YAG (neodymium-doped yttrium aluminium garnet) laser (355 nm) is used as the light source and the voltage of series resistor as a function of time is recorded by the oscilloscope (Figure S4, Supporting Information). The resistance of the sample decreases under the pulse laser with pulse duration of 3–5 ns irradiation leading to the rising of partial voltage on series resistor. The normalized voltage response as a function of time is shown in Figure 6d–f. The rise time and the fall time are defined as the time required for the  $I_{ph}$  to transition from 10 to 90% or drop from 90 to 10%, which are measured to be  $\approx 4.5 \mu\text{s}$  and  $\approx 2.84 \text{ ms}$  for individual self-powered Se/PANI PD at zero bias shown in Figure 6d and Table 1, respectively, much faster than that of previously reported self-powered ZnO/PANI and  $\text{TiO}_2/\text{PANI}$  photodetectors.<sup>[19,25]</sup> The rise time and the fall time of Se/PPy and Se/PEDOT PD under the pulse laser are about 0.35/16.97 ms (Figure 6e) and 1.00/9.78 ms, respectively (Figure 6f). The superior photosensitivity and ultrafast response

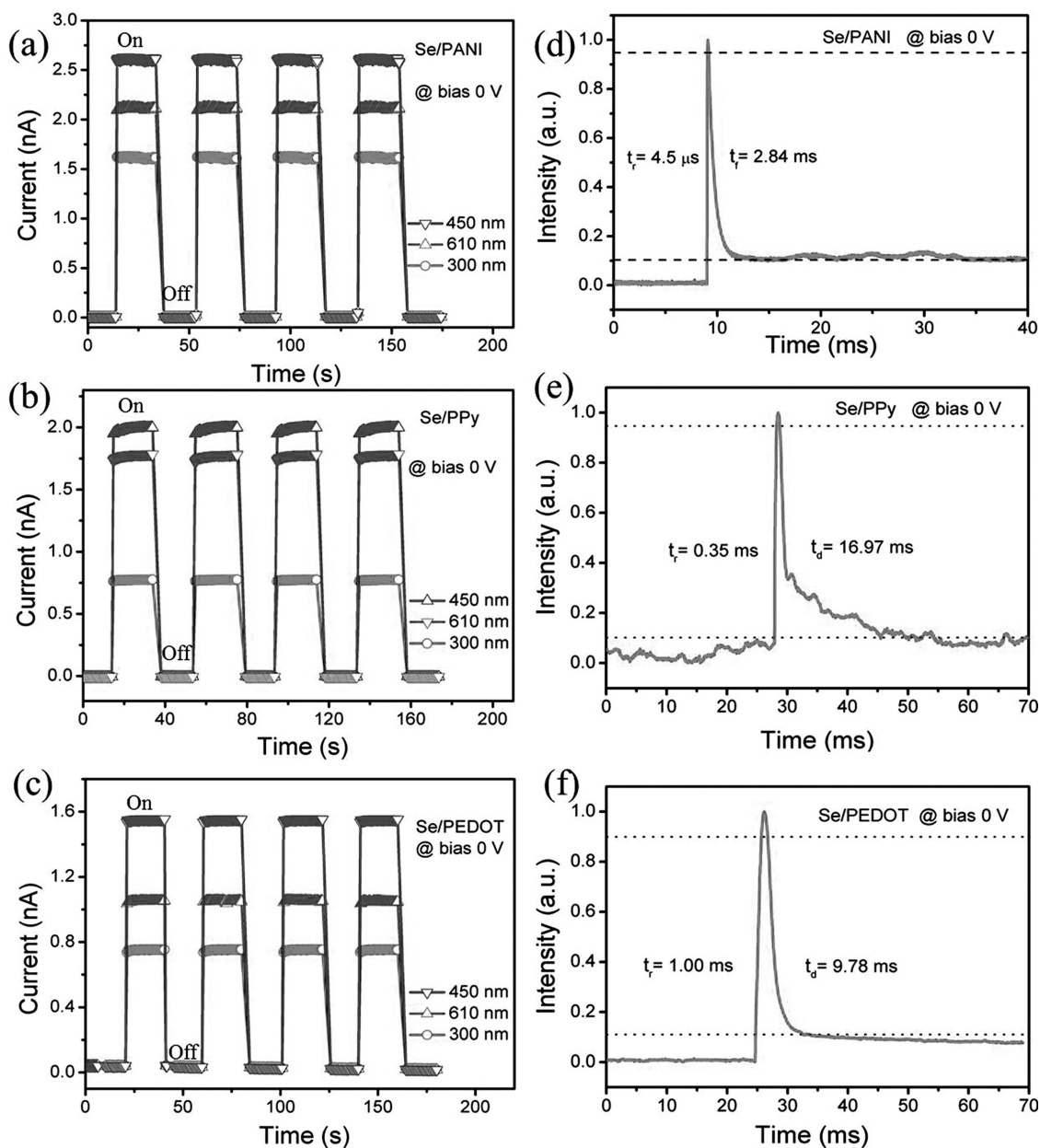


**Figure 6.** a–c)  $I$ - $t$  characteristics of Se/PANI, Se/PPy, and Se/PEDOT PDs under the dark and the 300-nm- ( $0.403 \text{ mW cm}^{-2}$ ), 450-nm- ( $1.003 \text{ mW cm}^{-2}$ ), and 610-nm- ( $0.434 \text{ mW cm}^{-2}$ ) light illumination, respectively, and d–f) their corresponding pulse response under 2 Hz 355-nm-pulse laser radiation.

speed of the three self-powered inorganic/organic heterojunction PDs are shown in Table 1, providing a good opportunity for developing future microscale photodetectors.

The spectral responsivity ( $R_\lambda$ ), external quantum efficiency (EQE), and detectivity ( $D^*$ ) are also key parameters in defining the performances of self-powered photodetectors. The spectra responsivity is defined by the following equation

$$R_\lambda = (I_{\text{ph}} - I_d) / P_\lambda S \quad (1)$$

$$\text{EQE} = R_\lambda \times hc / e\lambda \quad (2)$$

where  $P_\lambda$  is light power density and  $S$  is the effective illuminated area from measured data ( $1.25 \times 10^{-5} \text{ cm}^2$ ),  $\lambda$  is the light

wavelength,  $h$  is Planck's constant,  $e$  is the electronic charge, and  $c$  is the velocity of light.

The definition of detectivity ( $D^*$ ) can be calculated as the following equation

$$D^* = R_\lambda / (2qJ_d)^{1/2} \quad (3)$$

where  $q$  is the elementary electronic charge and  $J_d$  is the dark current density. As shown in Figure 7a–c, the responsivity of the three inorganic/organic photodetectors is observed in the UV and visible region, indicating a broadband photosensitivity. The maximum responsivity is consistent with the UV–vis absorption spectra of hybrid composites. It is clear that the

**Table 1.** Performance comparison of Se/conducting polymers photodetectors and other hybrid organic/inorganic photodetectors under zero bias.

Photodetector	Light and $P_\lambda$	$I_{ph}$	$R_\lambda$	Rise time	Decay time	Ref.
MgZnO/PANI	250 nm; 0.13 mW cm <sup>-2</sup>	15.4 pA	0.16 mA W <sup>-1</sup>	<0.3 s	<0.3 s	[14]
ZnO/PANI/ZnO	365 nm; 8W	≈1.4 μA	–	–	–	[19]
TiO <sub>2</sub> /PANI	365 nm; –	0.35 mA	–	–	–	[24]
TiO <sub>2</sub> /PANI/TiO <sub>2</sub>	365 nm; 8 W	≈0.8 μA	–	1 s	2 s	[25]
TiO <sub>2</sub> /PANI	320 nm; 0.87 mW cm <sup>-2</sup>	≈32 nA	5 mA W <sup>-1</sup>	3.8 ms	30.7 ms	[41]
PEDOT:PSS/SnO <sub>2</sub>	450 nm; –	0.87 μA	18.2 mA W <sup>-1</sup>	Several s	Several s	[6]
PEDOT:PSS/ZnO	325 nm; –	1.2 nA	–	–	–	[21]
TiO <sub>2</sub> /spiro-MeOTAD	410 nm; 75 μW cm <sup>-2</sup>	≈0.1 μA	10 mA W <sup>-1</sup>	0.12 s	0.06 s	[58]
Se/PANI	610 nm; 0.434 mW cm <sup>-2</sup>	≈2.5 nA	120 mA W <sup>-1</sup>	4.50 μs	2.84 ms	This work
Se/PPy		≈2.0 nA	70 mA W <sup>-1</sup>	0.35 ms	16.97 ms	
Se/PEDOT		≈1.6 nA	5.5 mA W <sup>-1</sup>	1.00 ms	9.78 ms	

spectra responsivity of Se/PANI PD shows the higher value of 120 mA W<sup>-1</sup> at the wavelength of 610 nm than that of Se/PPy (70 mA W<sup>-1</sup>) and Se/PEDOT PD (5.62 mA W<sup>-1</sup>), respectively. This value is much higher than that reported for graphene PDs (0.5 mA W<sup>-1</sup>),<sup>[50]</sup> and is comparable to those reported organic–inorganic hybrid PDs as shown in Table 1. This result confirms that coating p-type conducting polymer on individual Se-MT can enhance the photoperformance in the visible region. In addition, other two small peaks of Se/PANI PD locate at 450 and 300 nm with a responsivity of 67 and 70 mA W<sup>-1</sup>, respectively. The EQE of Se/PANI at 610 nm wavelength measured under zero bias voltage is 24% higher than that of Se/PPy and Se/PEDOT as shown in Figure S5 in the Supporting Information. Owing to the low dark current and high responsivity, the  $D^*$  of Se/PANI at the wavelength of 610 nm in Figure 7a is  $3.78 \times 10^{11}$  cm Hz<sup>1/2</sup> W<sup>-1</sup> (Jones) at zero bias, much higher than that of 2,4-bis[4-(*N,N*-dimethylamino)phenyl]squaraine nanowire/crystalline Si (c-Si) p–n heterojunctions ( $0.06$ – $0.45 \times 10^{11}$  Jones).<sup>[51]</sup> For the Se/PPy (Figure 7b) and Se/PEDOT PDs (Figure 7c), the detectivity value is  $2.21 \times 10^{11}$  and  $1.76 \times 10^{10}$  Jones due to the relatively high dark current and low responsivity.

The experimental results show that the p-type conducting polymers grown on the Se-MT surface can greatly improve the hybrid photodetector performance. To further understand the photoresponse characteristics, the mechanism has been investigated as the following. The electron affinities ( $\chi$ ) of t-Se-MT, PANI, PPy, and PEDOT are taken as 3.2, 2.87, 3.5, and 3.3 eV, respectively.<sup>[21,30,46,52]</sup> Compared with t-Se-MT ( $E_g = 1.77$  eV),<sup>[30]</sup> p-type conducting PANI, PPy, and PEDOT have the higher bandgap energies of 2.76 eV,<sup>[40,52]</sup> 2.50 eV,<sup>[42,46]</sup> and 2.0 eV,<sup>[21]</sup> respectively. After depositing the conducting organic polymers, there are two type band alignments: type-I heterojunction of Se/PANI PD and type-II heterojunction for Se/PPy and Se/PEDOT PD. Under light irradiation, the electron–hole pairs are mainly generated by the photoresponse of the pure t-Se-MT. Due to the built-in electric field formed by type-II heterojunction of Se/PPy (Figure 7e) and Se/PEDOT PD (Figure 7f), the photo-generated holes will migrate from the highest occupied molecular orbital (HOMO) of PPy and PEDOT to the valance band of t-Se-MT, and then the photogenerated electrons in the conductive band of p-type t-Se-MT transfer to the lowest unoccupied

molecular orbital (LUMO) of PPy and PEDOT, leading to the fast separation of electron–holes pairs to yield a photocurrent. Unlike the PPy and PEDOT whose heteroatoms contribute slightly to  $\pi$ -band formation, the alternating ring-heteroatom structures in the PANI backbone provide the different oxidation levels, including reduced leucoemeraldine base, conducting ES, and fully oxidized pernigraniline base.<sup>[53,54]</sup> The positively charged polarons in ES formed PANI give rise to a defect state at roughly 1.5 eV above HOMO level (Figure 7d),<sup>[55,56]</sup> thus the new type-II p–p heterojunction is formed. In addition, a portion of electrons in LUMO of PANI might be excited to the conductive band of t-Se-MT, and then migrate to the polaron band of PANI. This addition electron process can effectively suppress the electron–hole recombination in the conducting PANI, enhancing the photocurrent of Se/PANI. Moreover, the photoresponse decreases as the thickness of PANI layer in the hybrid devices increases (Figure S6, Supporting Information). Therefore, the p–p junction Se/PANI PD exhibits higher photocurrent, faster on/off response speed, and higher responsivity than Se/PPy and Se/PEDOT.

The photocurrent for individual Se/PANI PD as a function of 610 nm light intensity at zero bias voltage is presented in Figure 8a. Obviously, the photocurrent increases gradually with light intensity increasing from 0.147 to 0.542 mW cm<sup>-2</sup>. The nonlinear plot can be fitted to a power law,  $I \approx P^\theta$  ( $\theta = 0.78$ ), indicating a complex process of electron–hole generation, recombination and trapping at the Se/PANI interface.<sup>[57,58]</sup> The reproducibility of the self-powered PDs of individual Se/PANI, Se/PPy, and Se/PEDOT are also measured by repetitively recording of  $I$ – $t$  characteristics. Five PD devices are measured at zero bias voltage and the responsivity at 610 nm of Se/PANI, Se/PPy, and Se/PEDOT is  $120 \pm 10$ ,  $70 \pm 5$ , and  $5.5 \pm 0.5$  mA W<sup>-1</sup>, respectively (Figure 8b). The results indicate that the as-fabricated Se/conducting polymers PD devices have excellent reproducibility, suggesting a possible method to fabricate self-powered photodetectors with fast response speed.

### 3. Conclusion

In summary, three novel Se/PANI, Se/PPy, and Se/PEDOT heterojunctions were successfully fabricated by depositing

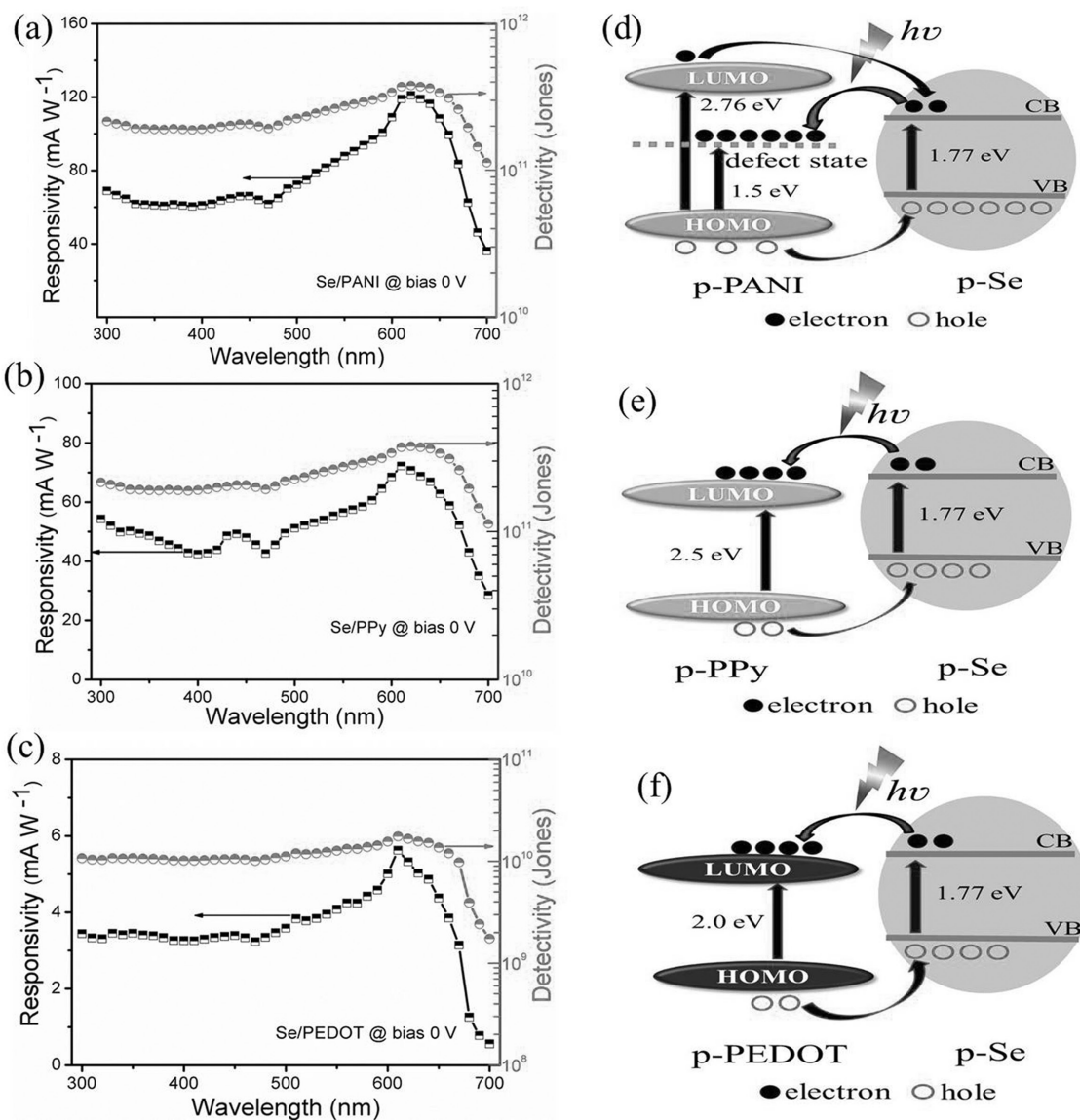


**Figure 7.** a–c) Spectra responsivity and detectivity characteristics of the Se/PANI, Se/PPy, and Se/PEDOT PDs with irradiance wavelength ranging from 300 to 700 nm under 0 V bias, respectively. Energy band diagrams for d) Se/PANI, e) Se/PPy, and f) Se/PEDOT heterojunctions.

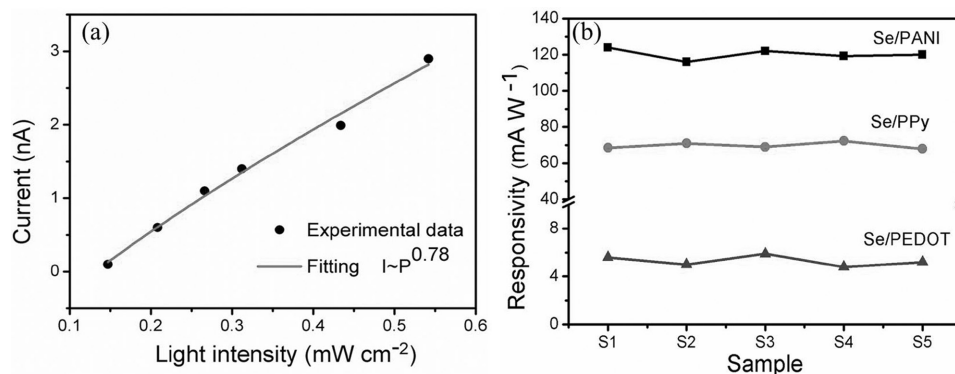


**Figure 8.** a) Photocurrent of Se/PANI PD versus light intensity and corresponding fitted curve using the power law under 610 nm light. b) The responsivity of five Se/PANI, Se/PPy, and Se/PEDOT devices under 610 nm at zero bias voltage.



PANI, PPy, and PEDOT films on single t-Se-MT through one-step in situ polymerization in acid solution. The as-prepared p-p heterojunctions can directly be used as photodetector to simplify the fabrication process, providing a simple and efficient approach to prepare high performance photodetectors. The three devices exhibit a self-powered UV-vis broadband response and ultrafast response speed. In particular, single Se/PANI PD with 45 nm thickness of PANI layer possesses a large photocurrent to dark current ratio of  $1.1 \times 10^3$ , high spectral responsivity ( $120 \text{ mA W}^{-1}$ ), good detectivity ( $3.78 \times 10^{11}$  Jones), and fast response speed (rise time of 4.5  $\mu\text{s}$  and fall time of 2.84 ms) at the very low visible light intensity illumination ( $0.434 \text{ mW cm}^{-2}$ , 610 nm) at zero bias voltage. The good photoresponse performance of t-Se-MT/conducting polymers photodetectors is attributed to the built-in electric field arising from p-p heterojunctions at the interface, which is beneficial to separating the electron-hole pairs and restraining the recombination in t-Se-MT for improving the photocurrent. Therefore, this approach is a promising way for fabricating other inorganic semiconductors and organic polymers heterojunctions for photodetector applications.

#### 4. Experimental Section

**Synthesis of t-Se-MTs:** The t-Se-MTs were synthesized by a vapor transport and deposition process in a horizontal tube furnace. In a typical process, Se source (>99.95%, Meixing Chemical Co., Ltd., Shanghai) serving as the source material was placed in the center of the furnace. Clean silicon substrate was placed 28 cm downstream from center vertically. The quartz tube was first flushed with ultrapure nitrogen for 30 min, and then the tube furnace was heated to 300 °C in 55 min and kept for 720 min with a constant nitrogen flow of 300 sccm. After the reaction, the growth of Se-MTs was obtained on a clean Si/SiO<sub>2</sub> wafer.

**Fabrication of Hybrid PDs:** An as-synthesized t-Se-MT was then transferred to a piece of glass without further treatment. One side of the single t-Se-MT was fixed on the glass using the Indium electrode, and then the whole glass was immersed into the 0.1 M H<sub>2</sub>SO<sub>4</sub> (10 mL) cold aqueous solution containing a given amount of aniline, pyrrole or 3,4-ethylenedioxythiophene monomer for 1 h, followed by rapidly adding 10 mL 0.1 M H<sub>2</sub>SO<sub>4</sub> cold aqueous solution containing ammonium peroxydisulfate (22.82 mg) into the above mixture. The mixture was slightly stirred for 5 min and the polymerization was carried out at 0 °C for overnight. After polymerization, the sample was washed by deionized water and ethanol and dried at 60 °C. The different thickness of PANI layer is controlled by the polymerization time. Indium electrode was used to fix the other side of Se/PANI, Se/PPy or Se/PEDOT to construct a self-powered PD. The other five PDs based on above Se/conducting polymers were fabricated under the same experiment condition.

**Materials Characterization:** Morphologies of t-Se-MT and heterojunctions were investigated by a field-emission scanning electron microscopy (Zeiss Sigma). Crystallinity and compositions of the t-Se-MT/conducting polymers were characterized by XRD (Bruker D8-A25) using Cu K $\alpha$  radiation ( $\lambda = 0.15406 \text{ nm}$ ) in the  $2\theta$  range from 20° to 65°, Raman spectroscopy (LabRam-1B, He-Ne laser excitation at 632.8 nm for 10 s), and XPS (PHI 5000C ESCA) using a monochromatic Al X-ray source (97.9 W, 1486.6 eV). The optical properties of t-Se-MT/conducting polymers were characterized by a UV-vis spectrophotometer (Hitachi U-3900H).

**Photoelectric Measurement:** The I-V and I-t characteristics and spectral photoresponses of the hybrid photodetectors were measured by a semiconductor characterization system (Keithley 4200-SCS), a 24 W Xe lamp (POWERMAX II P21NRX3), and monochromators. Time resolved responses of the device were measured via the circuit including with a

Nd:YAG laser with pulse duration of 3–5 ns (Continuum Electro-Optics, MINILITE II, 355 nm), oscilloscope (Tektronix MSO/DPO5000), and a 1 G $\Omega$  resistor.

#### Supporting Information

Supporting Information is available from the Wiley Online Library or from the author.

#### Acknowledgements

This work was financially supported by the National Natural Science Foundation of China (Grant Nos. 11674061 and 51471051), Science and Technology Commission of Shanghai Municipality (Grant No. 15520720700), Postdoctoral Science Foundation of China (Grant No. 2015M571486), Shanghai Shu Guang Project (Grant No. 12SG01), and the Programs for Professor of Special Appointment (Eastern Scholar) at Shanghai Institutions of Higher Learning, part of the experimental work has been carried out in Fudan Nanofabrication Laboratory.

#### Conflict of Interest

The authors declare no conflict of interest.

#### Keywords

polyaniline, polypyrrole, poly(3,4-ethylenedioxythiophene), selenium, self-powered photodetectors

Received: June 12, 2017  
Revised: July 11, 2017  
Published online: August 4, 2017

- [1] H. Y. Chen, H. Liu, Z. M. Zhang, K. Hu, X. S. Fang, *Adv. Mater.* **2016**, *28*, 403.
- [2] J. Zhou, L. Chen, Y. Wang, Y. He, X. Pan, E. Xie, *Nanoscale* **2016**, *8*, 50.
- [3] M. S. Zhu, Y. Huang, Y. Huang, Z. X. Pei, Q. Xue, H. F. Li, H. Y. Geng, C. Y. Zhi, *Adv. Funct. Mater.* **2016**, *26*, 4481.
- [4] L. Peng, L. Hu, X. S. Fang, *Adv. Funct. Mater.* **2014**, *24*, 2591.
- [5] L. X. Zheng, K. Hu, F. Teng, X. S. Fang, *Small* **2017**, *13*, 1602448.
- [6] S. Li, S. Wang, K. Liu, N. Zhang, Z. Zhong, H. Long, G. Fang, *Appl. Phys. A* **2015**, *119*, 1561.
- [7] B. Zhao, F. Wang, H. Y. Chen, L. X. Zheng, L. X. Su, D. X. Zhao, X. S. Fang, *Adv. Funct. Mater.* **2017**, *27*, 1700264.
- [8] H. Y. Yang, D. I. Son, T. W. Kim, J. M. Lee, W. I. Park, *Org. Electron.* **2010**, *11*, 1313.
- [9] L. Z. Hao, Y. J. Liu, W. Gao, Z. D. Han, Z. J. Xu, Y. M. Liu, J. Zhu, *RSC Adv.* **2016**, *6*, 40192.
- [10] Q. Li, S. Ding, W. Zhu, L. Feng, H. Dong, W. Hu, *J. Mater. Chem. C* **2016**, *4*, 9388.
- [11] J. Gao, Y. Yang, Z. Zhang, J. Yan, Z. Lin, X. Guo, *Nano Energy* **2016**, *26*, 123.
- [12] M. Kalisz, S. Golczak, E. Frackowiak, K. Langer, J. J. Langer, *J. Mater. Chem. C* **2016**, *4*, 6634.
- [13] X. Yu, H. Yin, H. Li, W. Zhang, H. Zhao, C. Li, M. Zhu, *Nano Energy* **2017**, *34*, 155.
- [14] H. Y. Chen, P. Yu, Z. Zhang, F. Teng, L. Zheng, K. Hu, X. S. Fang, *Small* **2016**, *12*, 5809.

- [15] A. Varela-Álvarez, J. A. Sordo, G. E. Scuseria, *J. Am. Chem. Soc.* **2005**, *127*, 11318.
- [16] N. S. Sariciftci, L. Smilowitz, Y. Cao, A. J. Heeger, *J. Chem. Phys.* **1993**, *98*, 2664.
- [17] Y. H. Kim, C. Foster, J. Chiang, A. J. Heeger, *Synth. Met.* **1988**, *26*, 49.
- [18] J. R. Cárdenas, E. A. de Vasconcelos, W. M. de Azevedo, E. F. da Silva, I. Pepe, A. F. da Silva, S. S. Ribeiro, K. A. Silva, *Appl. Surf. Sci.* **2008**, *255*, 688.
- [19] S. Yang, J. Gong, Y. Deng, *J. Mater. Chem.* **2012**, *22*, 13899.
- [20] Y. Oaki, T. Oki, H. Imai, *J. Mater. Chem.* **2012**, *22*, 21195.
- [21] P. Lin, X. Yan, Z. Zhang, Y. Shen, Y. Zhao, Z. Bai, Y. Zhang, *ACS Appl. Mater. Interfaces* **2013**, *5*, 3671.
- [22] S. Yang, S. Tongay, S.-S. Li, J.-B. Xia, J. Wu, J. Li, *Appl. Phys. Lett.* **2013**, *103*, 143503.
- [23] X. Wang, W. Song, B. Liu, G. Chen, D. Chen, C. Zhou, G. Shen, *Adv. Funct. Mater.* **2013**, *23*, 1202.
- [24] H. Wang, G. Yi, X. Zu, X. Jiang, Z. Zhang, H. Luo, *Mater. Lett.* **2015**, *138*, 204.
- [25] X. Zu, H. Wang, G. Yi, Z. Zhang, X. Jiang, J. Gong, H. Luo, *Synth. Met.* **2015**, *200*, 58.
- [26] V. W. Yam, Q. Li, *Chem. Commun.* **2006**, *9*, 1006.
- [27] B. Zhang, W. Dai, X. Ye, F. Zuo, Y. Xie, *Angew. Chem.* **2006**, *118*, 2633.
- [28] S. Y. Zhang, Y. Liu, X. Ma, H. Y. Chen, *J. Phys. Chem. B* **2006**, *110*, 9041.
- [29] J. Zhang, Y. Xu, L. Fan, Y. Zhu, J. Liang, Y. Qian, *Nano Energy* **2015**, *13*, 592.
- [30] K. Hu, H. Y. Chen, M. M. Jiang, F. Teng, L. X. Zheng, X. S. Fang, *Adv. Funct. Mater.* **2016**, *26*, 6641.
- [31] E. Filippo, D. Manno, A. Serra, *Chem. Phys. Lett.* **2011**, *510*, 87.
- [32] E. Filippo, D. Manno, A. Serra, *Cryst. Growth Des.* **2010**, *10*, 4890.
- [33] P. Yu, X. Zhao, Z. Huang, Y. Li, Q. Zhang, *J. Mater. Chem.* **2014**, *2*, 14413.
- [34] P. Yu, Y. Li, X. Zhao, L. Wu, Q. Zhang, *Langmuir* **2014**, *30*, 5306.
- [35] N. Jabeen, Q. Xia, M. Yang, H. Xia, *ACS Appl. Mater. Interfaces* **2016**, *8*, 6093.
- [36] D. Wei, X. Lin, L. Li, S. Shang, M. C. W. Yuen, G. Yan, X. Yu, *Soft Matter* **2013**, *9*, 2832.
- [37] F. Wang, X. Zhan, Z. Cheng, Z. Wang, Q. Wang, K. Xu, M. Safdar, J. He, *Small* **2015**, *11*, 749.
- [38] J. Zhang, X. S. Zhao, *J. Phys. Chem. C* **2012**, *116*, 5420.
- [39] P. Tang, L. Han, L. Zhang, *ACS Appl. Mater. Interfaces* **2014**, *6*, 10506.
- [40] L. X. Zheng, P. Yu, K. Hu, F. Teng, H. Chen, X. S. Fang, *ACS Appl. Mater. Interfaces* **2016**, *8*, 33924.
- [41] M. Canales, J. Torras, G. Fabregat, A. Meneguzzi, C. Aleman, *J. Phys. Chem. B* **2014**, *118*, 11552.
- [42] H. Ullah, A. U. H. A. Shah, S. Bilal, K. Ayub, *J. Phys. Chem. C* **2014**, *118*, 17819.
- [43] T. Abdiryim, A. Ali, R. Jamal, Y. Osman, Y. Zhang, *Nanoscale Res. Lett.* **2014**, *9*, 89.
- [44] P. P. Yu, Y. Z. Li, X. Zhao, L. H. Wu, Q. H. Zhang, *Synth. Met.* **2013**, *185*, 89.
- [45] L. Zhang, R. Jamal, Q. Zhao, M. Wang, T. Abdiryim, *Nanoscale Res. Lett.* **2015**, *10*, 148.
- [46] W. Zheng, X. Li, C. Dong, X. Yan, G. He, *RSC Adv.* **2014**, *4*, 44868.
- [47] B. Anothumakkool, R. Soni, S. N. Bhange, S. Kurungo, *Energy Environ. Sci.* **2015**, *8*, 1339.
- [48] G. P. Pandey, A. C. Rastogi, *Electrochim. Acta* **2013**, *87*, 158.
- [49] J. M. Ginder, A. J. Epstein, *Phys. Rev. B* **1990**, *41*, 10674.
- [50] F. Xia, T. Mueller, Y. M. Lin, A. Valdes Garcia, P. Avouris, *Nat. Nanotechnol.* **2009**, *4*, 839.
- [51] W. Deng, J. Jie, Q. Shang, J. Wang, X. Zhang, S. Yao, Q. Zhang, X. Zhang, *ACS Appl. Mater. Interfaces* **2015**, *7*, 2039.
- [52] A. A. Hussain, B. Sharma, T. Barman, A. R. Pal, *ACS Appl. Mater. Interfaces* **2016**, *8*, 4258.
- [53] S. Stafstrom, J. L. Bredas, A. J. Epstein, H. S. Woo, D. B. Tanner, W. S. Huang, A. G. MacDiarmid, *Phys. Rev. Lett.* **1987**, *59*, 1464.
- [54] M. G. Roe, J. M. Ginder, P. E. Wigen, A. J. Epstein, M. Angelopoulos, A. G. MacDiarmid, *Phys. Rev. Lett.* **1988**, *60*, 2789.
- [55] R. P. McCall, J. M. Ginder, J. M. Leng, H. J. Ye, S. K. Manohar, J. G. Masters, G. E. Asturias, A. G. MacDiarmid, A. J. Epstein, *Phys. Rev. B* **1990**, *41*, 5202.
- [56] I. A. Misurkin, T. S. Zhuravleva, V. M. Geskin, V. Gulbinas, S. Pakalnis, V. Butvilos, *Phys. Rev. B* **1994**, *49*, 7178.
- [57] E. Shalev, E. Oksenberg, K. Rechav, R. Popovitz Biro, E. Joselevich, *ACS Nano* **2017**, *11*, 213.
- [58] Y. Xie, L. Wei, Q. Li, G. Wei, D. Wang, Y. Chen, J. Jiao, S. Yan, G. Liu, L. Mei, *Appl. Phys. Lett.* **2013**, *103*, 261109.